Examining Asphaltene Solubility on Deposition in Model Porous Media

Yu-Jiun Lin[1], Peng He[1], Mohammad Tavakkoli[1], Nevin Thunduvila Mathew[2],

Yap Yit Fatt[3], John C. Chai[4], Afshin Goharzadeh[3], Francisco M. Vargas[1], and Sibani Lisa Biswal[1*]

*Author for correspondence

[1] Department of Chemical and Biomolecular Engineering, Rice University, Houston, TX, USA

[2] Department of Chemical Engineering, The Petroleum Institute, Abu Dhabi, United Arab Emirates

[3] Department of Mechanical Engineering, The Petroleum Institute, Abu Dhabi, United Arab Emirates

[4] School of Computing and Engineering, University of Huddersfield, UK

Corresponding Author Email: biswal@rice.edu

Abstract

Asphaltenes are known to cause severe flow assurance problems in the near-wellbore region of oil reservoirs. Understanding the mechanism of asphaltene deposition in porous media is of great significance for the development of accurate numerical simulators and effective chemical remediation treatments. Here, we present a study of the dynamics of asphaltene deposition in porous media using microfluidic devices. A model oil containing 5 wt% dissolved asphaltenes was mixed with *n*-heptane, a known asphaltene precipitant, and flowed through a representative porous media microfluidic chip. Asphaltene deposition was recorded and analyzed as a function of solubility, which was directly correlated to particle size and Péclet number. In particular, pore-scale visualization and velocity profiles, as well as three stages of deposition, were identified and examined to determine the important convection-diffusion effects on deposition.

Keywords: asphaltene deposition, model oil, microfluidic channels, porous media

Introduction

Asphaltenes have been referred to as the "cholesterol of petroleum"[1] because they can precipitate out of crude oils and plug pipelines.[2] Recently, of particular interest is asphaltene deposition in the near-wellbore region, which represents the porous media of reservoir rock near the wellbore tubing and casing. By understanding the asphaltene deposition dynamics in porous media, especially at the pore scale, better oil flow processes can be designed.

Generally, asphaltenes are defined as the species in crude oils that are soluble in aromatics (i.e., toluene) and insoluble in *n*-alkanes (i.e., *n*-heptane).[3] The specific molecular structure of asphaltene molecules typically cannot be uniquely defined due to their general classification based on solubility. Theoretically, various equations of state or mixing free energy models, such as Flory-Huggins theory, have been utilized to describe the solubility and oil-asphaltene bulk-phase equilibria.[3–5] Experimentally, refractive index measurements have been used to describe changes in the solubility of asphaltene.[6,7] If the pressure, temperature, or composition of crude oil are varied, the solubility parameter of asphaltenes will be altered, and the asphaltenes can be destabilized to precipitate and aggregate out of the oil, causing deposition problems in pipelines and porous media.[8,9]

Numerous studies have examined the arterial deposition of asphaltenes in glass and stainless steel capillary pipes.[7,10–16] Diffusion is typically assumed to be an important mechanism leading to asphaltenes deposition. Nabzar *et al*. proposed a colloidal model for asphaltene deposition in the diffusion-limited and shear-limited regimes.[10] Vargas *et al.* proposed that there is a competition between the flocculation and deposition of asphaltenes in well production.[17] It is believed that asphaltenes will either aggregate to form large colloidal systems that can readily flow through a pipe or deposit onto the surface. Asphaltene deposition in porous media has been

less investigated, and various deposition mechanisms such as hydrodynamic bridging must be considered. Coreflood tests have been widely utilized to analyze the effects of miscible and immiscible fluid injections on permeability impairment and formation damage.[18] However, only macroscopic properties, such as the permeability reduction due to asphaltene deposition, can be obtained; the dynamics of asphaltene precipitation and deposition within porous media have not been visualized at the pore scale.

Recently, microfluidic devices have been utilized to provide insight into oil flow processes.[19,20] Asphaltene contents in crude oil samples have been characterized using glass microfluidic devices.[21,22] A microfluidic packed bed reactor has been utilized to study the kinetics of asphaltene deposition and dissolution in a porous media system.[23,24] A detailed understanding of how their solubility influences the deposition of asphaltenes at the pore scale has not been studied. Here, we investigate the dynamics of asphaltene deposition after destabilization by the precipitant of *n*-heptane in a microfluidic channel of porous media by high-speed optical microscopy. Model oil with a known asphaltene content is utilized in the experiments because other intrinsic components in crude oil are known to influence asphaltene stability.[25–27] The solubility parameter of the oil-precipitant mixture is used to generalize the effects of precipitant concentration with respect to the model oil. The resulting asphaltene aggregates are further identified by their Péclet number for the analysis of deposition dynamics. The deposition rate is found to vary nonlinearly with precipitant fractions. The pressure drop across the porous media is measured to correlate the deposition dynamics with the decrease in permeability. The velocity and shear rate profiles within the pore are obtained to explain the pore-scale dynamic deposition process based on the convection-diffusion effect.

The remainder of this article is divided into three (3) sections. Background preparations for carrying out the experiments are discussed in the next section, followed by presentations and discussions of the experimental observations and the associated calculations. Finally, concluding remarks are presented.

Materials and Methods

All chemicals were of reagent grade (purity ≥ 95%), purchased from Sigma-Aldrich and used without further purification.

Preparation and Characterization of Model Oil

In this study, a model oil composed of toluene and asphaltenes was used in the experiments to reduce the effects of complex components typically found in the crude oil. The asphaltenes used in this research were extracted by *n*-pentane from bitumen samples from the Middle East with an asphaltene concentration greater than 20 wt%. The extracted asphaltenes were then slowly dissolved in toluene at 90^{o}C in a 40 kHz ultrasonic bath (VWR) for a minimum of 30 minutes until a final asphaltene concentration of 5 wt% was achieved. Determining asphaltene precipitation is a key step prior to studying asphaltene aggregation and deposition. The amount of precipitated asphaltenes after mixing with *n*-heptane was measured using the "indirect method", a combination of gravimetric and spectroscopic techniques described by Tavakkoli *et al.*,[28] shown in Figure 1.

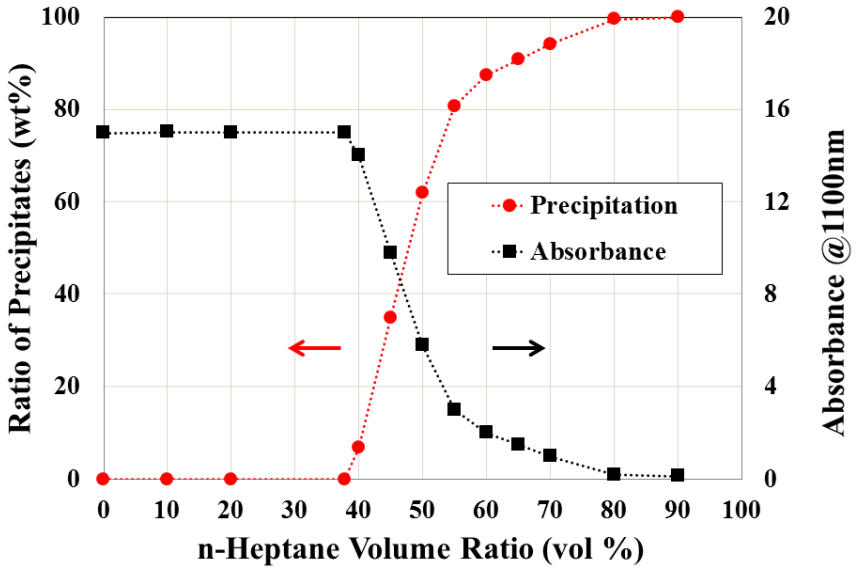

Figure 1: Asphaltene precipitation ratio results from the indirect method for the model oil mixed with *n*-heptane. Precipitation onset occurs at 37.74 vol% of *n*-heptane. The average standard deviation (ASD) of absorbance is 1.74%. (■) Absorbance at 1100 nm. (●) Ratio of precipitation.

To generalize the properties of the oil-precipitant mixture, the solubility parameter following the volumetric mixing rule is used. The solubility parameter was derived by Hildebrand and defined as the square root of the cohesive energy density.[29] Changing the solubility parameter alters the interactive forces between asphaltenes. Several groups have adopted the solubility parameter to describe the properties of oil-precipitant-solvent systems.[30–32] The solubility parameter of the model oil was measured and calculated from its refractive index. Refractive indices were measured by a refractometer (Anton Paar WR) at the wavelength of the sodium D line (589.3 nm) with an accuracy of ± 1×10^{-4} nD and over a measuring range of 1.30 to 1.72 nD. The solubility parameter for each volume ratio of *n*-heptane was found to vary from 17.01 $MPa^{0.5}$ at 40 vol% to 15.8 $MPa^{0.5}$ at 80 vol% (see Supplementary Figure S1 and Table S1).

Experimental Setup for Asphaltene Deposition

All experiments were performed under ambient conditions at a fixed temperature of 23°C. The model oil and precipitant (*n*-heptane) were injected separately by syringe pumps (Harvard

Apparatus PHD 2000), mixing at a T-junction (IDEX, MicroTee Assembly PEEK-1/16 in), and the mixture subsequently flowed through the porous media microchannel, where the asphaltene deposition was observed via optical microscopy. The total flow rate of the fluid mixture was fixed at $Q = 60$ μL/min, which corresponds to an equivalent superficial velocity of $u = 0.028$ m/s. The volume fraction of *n*-heptane in the mixture, $\varphi_h = Q_{heptane}/Q$, varied from 40% to 80%. The experimental time t at different values of φ_h also varied from 10 to 30 minutes such that the total oil injection volume $V_{oil} = (1 - \varphi_h)Qt$ remained constant. The microfluidic device was staged on an inverted microscope (Olympus IX 71), as shown in Figure 2a, and the deposition process was recorded using a high-speed CMOS camera (Phantom V4.3, Vision Research, Inc.). A differential pressure transducer (Validyne P610) was connected to the microchannel to measure the pressure drop across the porous media.

Design and Fabrication of Porous Media Microchannel

To mimic the porous media of the near-wellbore region, a homogeneous pore network of circles was designed such that the diameter of the circular posts and the smallest pore-throat spacing were both 125 μm, as shown in Figure 2b. All microfluidic devices were made of NOA-81 (Norland Optical Adhesive), a thiolene photopolymer with known solvent resistance and temperature tolerance.[33,34] Standard lithography protocols were followed to fabricate a SU-8 2015 (Microchem Corp) photoresist template that was a 20 micron tall negative relief of the porous media pattern. Then, a liquid polydimethylsiloxane (PDMS) (Sylgard 184, Dow Corning), mixed in a 10:1 ratio of elastomer base to curing agent, was poured onto the SU-8 mold, cured at 60°C, and removed to form a negative relief. NOA-81 was subsequently poured on the negative relief as well as a blank PDMS layer, and both were cured under a UV lamp. Both the NOA-81 porous media patterned layer and blank NOA-81 base were then released from the PDMS layer.

The blank NOA-81 base was mounted on a clean glass slide. The patterned NOA-81 layer and blank base were bonded by treating with O_2 plasma.[35] A representative microfluidic device with the corresponding fittings is shown in Figure 2c. The length of the porous media (L_p) is 10 mm. The permeability of the micromodel is approximately 5.23 Darcy, similar to that of a sand pack or a gravel pack.[36] The surface contact angle of the NOA microchannel was 79.50º±2.67, making the channel slightly water-wet, as measured by the sessile drop method (KSA CAM 200). The devices were used only once per experiment.

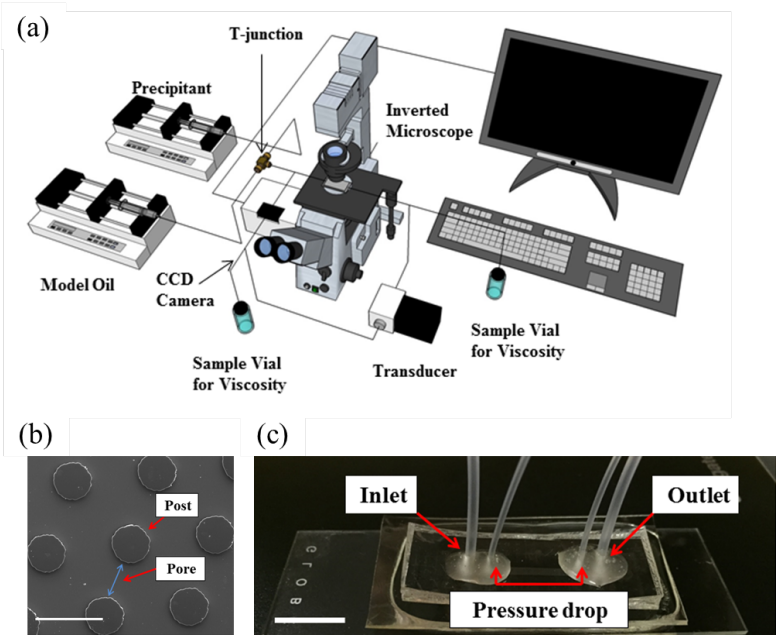

Figure 2: (a) Schematic of experimental setup. (b) SEM image of the porous media used to study deposition. (c) A complete NOA-81 microchannel. The white scale bars represent (b) 200 µm and (c) 1.0 cm.

Data Analysis

The experimental images were processed using ImageJ[37] and the Python image-processing module scikit-image.[38] First, the location of each post in the porous media was identified by image registration, and the pixel count associated with asphaltene deposition around each post

was determined by image thresholding using Otsu's method.[39] Next, the pixel count was converted to a coverage area and multiplied by the microchannel height, $h = 20$ μm, to obtain an average asphaltene deposition volume. The mass of deposition, m_d, was calculated by multiplying the deposition volume by the average asphaltene density $\rho = 1200$ kg/m^3. Finally, the average deposition over multiple posts was determined. Note that this calculation assumes that asphaltene deposition spanned across the microchannel.

Results and Discussions

Deposition Rate of Asphaltenes in Porous Media

Representative images of asphaltene deposition for varying *n*-heptane volume fractions at a fixed injection volume are shown in Figure 3. The flow occurred from left to right and the front (left) side of the post made first contact with the incoming fluid mixture. The particle size distribution (PSD) was obtained by dynamic light scattering (DLS) measurements (see Supplementary Figure S2). At *n*-heptane volume fractions φ_h < 50%, submicron asphaltene aggregates were observed. Upon increasing φ_h, the mean aggregate size increased, and micron-sized aggregates dominated at φ_h > 65%. The PSD was further used to calculate the range of Péclet numbers, using Eqns. 1-2, for each volume fraction to compare the relative ratios of convection to diffusion (See Supplementary Table S1).

$$\mathrm{Pe} = \frac{2uR_p}{D_{BM}} \tag{1}$$

$$\mathrm{D}_{BM} = \frac{k_B T}{6\pi\mu R_p} \tag{2}$$

R_p is the particle radius (~100–1000 nm), D_{BM} is the Brownian diffusivity (m^2/s), $u = 0.028$ m/s is the superficial velocity, μ is the dynamic viscosity of the fluid (~0.42–0.51 cP), and $k_B =$

1.38×10^{-23} $(m^2 \cdot kg)/(s^2 \cdot K)$ is the Boltzmann constant. A range of Péclet numbers is provided to illustrate the relative contributions of convection and diffusion, whereby convection becomes more dominant at high φ_h. Optical microscopy images show that when φ_h > 50%, asphaltenes were deposited on each post in a cone-like pattern against the direction of fluid flow, as shown in Figure 3a. At higher φ_h, the cone shape continued to be a characteristic of the deposition pattern ahead of each post, and deposition on the backside of the post was observed. Of particular interest is the variation in the aspect ratio of the cone shape. At φ_h > 70%, significant bridging was observed between the posts, as shown in Figure 3e. For φ_h = 40%, an insignificant amount of deposition of the submicron aggregates was observed (data not shown).

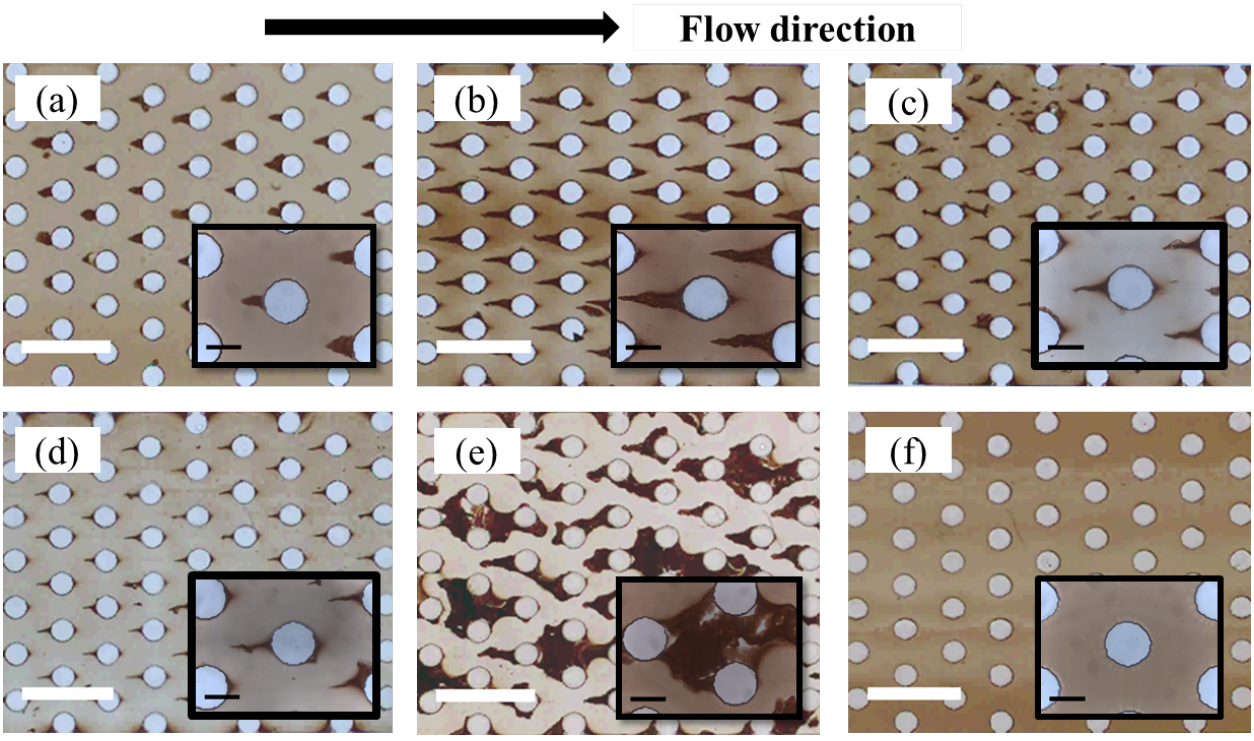

Figure 3: Images of asphaltene deposition in homogeneous porous media. (a) 50, (b) 55, (c) 60, (d) 65, (e) 70, and (f) 0 vol% *n*-heptane. Flow occurred from left to right. The white scale bar is 500 μm, and the black scale bar is 100 μm. The vol% of *n*-heptane altered the mean asphaltene aggregate size, which altered the relative ratio of convection to diffusion, as characterized by the range of Péclet numbers (Pe) (a) Pe = 1.9×10^4 - 1.3×10^5, (b) Pe = 3.3×10^4 - 5.2×10^5, (c) Pe = 2.3×10^4 - 1.9×10^6, (d) Pe = 9.3×10^4 - 1.8×10^6, and (e) Pe = 1.5×10^5 - 2.8×10^6.

The mass ratio of deposited asphaltenes versus precipitated asphaltenes was used to quantify the asphaltene deposition rate, $\dot{m}_d$. Figure 4a shows the deposition mass m_d (in μg) with respect to the precipitated asphaltenes mass m_i (in mg) in the mixtures passing through. For each φ_h, the total asphaltene content in the model oil and the ratio of precipitates (Figure 1) remained constant; hence, m_i increased linearly with time, $m_i = \dot{m}_i t$, and $\dot{m}_d$ was obtained from a linear regression of the m_d–m_i curve (Figure 4a). As previously described, the onset of precipitation occurred at a *n*-heptane volume fraction φ_{onset} = 37.74%, above which asphaltenes began to precipitate into submicron- or micron-sized aggregates due to decreased solubility.[26] Because φ_h = 40% was just above the onset point, the aggegates were nanosized; therefore, the time required to form deposits far exceeded the residence time in our microfluidic channel. Interestingly, between φ_h= 40 and 65%, the deposition rate increased and then decreased. It has been reported that the structure of the precipitates shifts from that of nanoaggregates to that of fractal-like micron-sized aggregates[26], in which case there is a competition between deposition and convection within the fluid. Finally, the deposition rate increased again from φ_h = 70 to 80% due to the increasing size of the asphaltene aggregates. Moreover, at φ_h > 70%, deposition occurred rather rapidly due to bridging between the posts. The measured pressure drop across the porous media increased as a result of the reduced permeability by asphaltene deposits (see Supplementary Figure S3). Overall, three stages of asphaltene deposition could be identified as a function of the Péclet number (Pe): 0 - 55% (small Pe, diffusion-dominated), 55 - 65% (intermediate Pe, shear removal), and 70 - 80% (large Pe, bridging). A detailed analysis of the deposition dynamics around a single post is discussed in the following section.

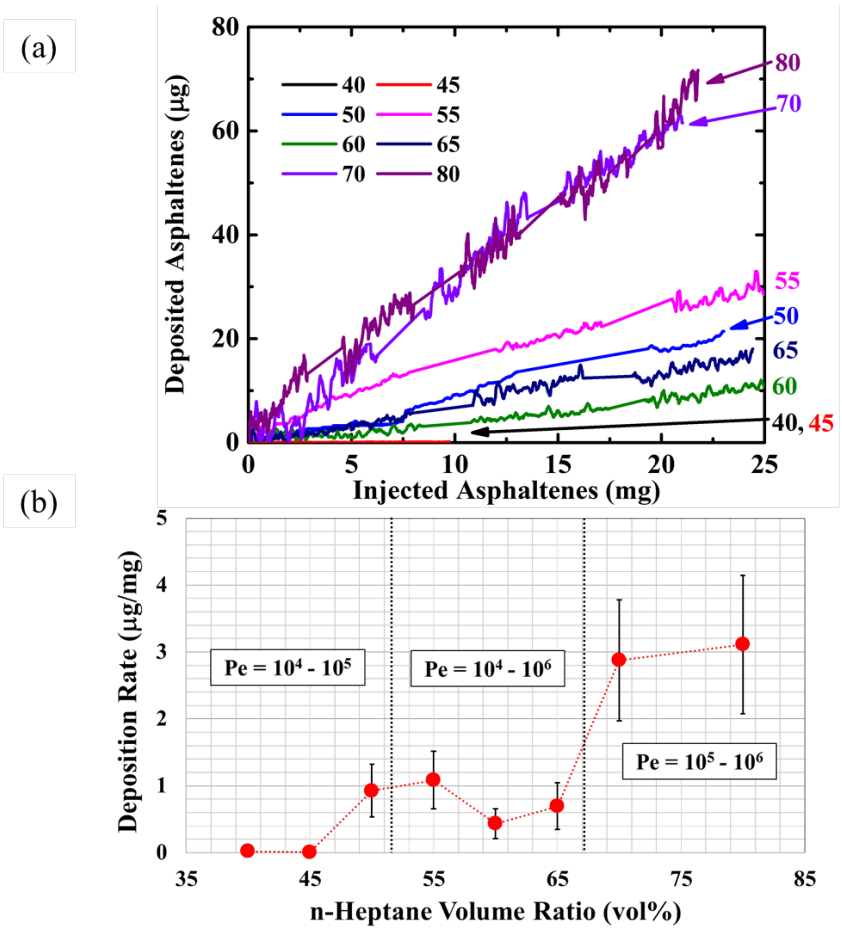

Figure 4: (a) Asphaltene deposition at different volume ratios of *n*-heptane. We assumed the average density of asphaltenes was 1200 kg/m^3. (b) Asphaltene deposition rate (μg/mg), which is the slope of the linear fitting from (a) versus the concentration of *n*-heptane (vol%) at the corresponding Péclet number.

Dynamics of Asphaltene Deposition onto a Post

The asphaltene deposition observed is characteristic of particle deposition profiles previously observed with micron-sized latex particles around a single cylindrical post by varying the Péclet number.[40] At φ_h =50%, the deposited asphaltenes adopted a broad cone-like shape (Pe = 1.9 × 10^4 - 1.3 × 10^5, Figure 5a). Submicron asphaltene aggregates more readily deposited in the stagnation region of the post and grew against the direction of flow via convection and diffusion. The cone elongated and narrowed at φ_h = 55% (Pe = 3.3 × 10^4 - 5.2 × 10^5, Figure 5b). The cone was blunted and shortened due to a competition between deposition and erosion at φ_h = 60% (Pe

= 2.3 × 10^4 - 1.9 × 10^6, Figure 5c). Vincent *et al.* observed a similar deposition profile with micron-sized polystyrene colloids under various convection-diffusion conditions.[41] Finally, at φ_h = 70 - 80% (Pe = 10^5 - 10^6), bridging of the asphaltene deposits across posts occurred among larger asphaltene aggregates. As soon as bridging occurred, precipitated asphaltenes continued to be entrained. Hu *et al*. showed that mechanical entrapment is the dominant mechanism for insoluble asphaltene deposition in a packed-bed device.[23,24]

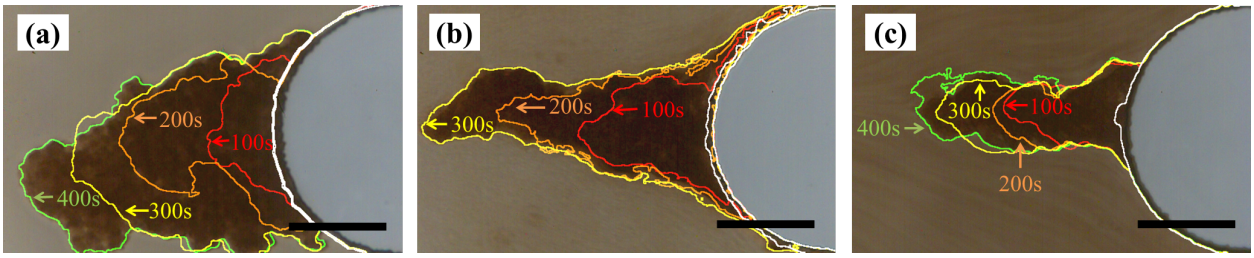

Figure 5: Dynamics of deposition growth at pore scale. (a) Cone-like, 50 vol% heptane; (b) finger-like, 55 vol% heptane; and (c) tip-like, 60 vol% heptane. The white, red, orange, yellow, and green lines represent the following times: initial stage, 100 s, 200 s, 300 s, and 400 s, respectively. The scale bar is 50 μm.

The dynamics of the deposition growth were governed by the relative contributions of convection and diffusion. The deposition profiles for the asphaltene aggregate at various times are shown in Figure 5. The profile for φ_h = 50% shows that the deposition grew against the fluid flow and broadened laterally, forming a characteristic wide, cone-like deposit. With increasing Péclet number, the deposition profiles became elongated and narrower at φ_h = 55% as deposition occurred more extensively in the stagnation region of the flow. The deposition tendency dominated erosion, resulting in the highest deposition rate. Furthermore, in the first stage (φ_h = 0 - 55%), the deposition rate also increased with more precipitated asphaltenes due to the lower solubility of the mixture. At this stage, the removal effect was not significant due to the relatively small Péclet number. Previous studies have also indicated that submicron aggregates are the

main determinants of surface deposition.[11,17,42] At φ_h = 60%, a blunt-tipped deposit was observed due to a balance between deposition and erosion.

The velocity and shear profiles around a characteristic asphaltene deposit on a single post for φ_h = 50, 55 and 60% were simulated using the lattice Boltzmann method (described in Supplementary Section S5) and are plotted in Figure 6 to better elucidate the local flow patterns around the deposited asphaltenes. The deposition grew in the stagnation region (shown in blue) at the centerline of the deposit against the fluid flow direction. The areas of highest shear rates (shown in red) occurred at the edges of the deposit. Hence, there was competition between deposition and shear removal, resulting in the cone-like deposition profiles. Furthermore, asphaltene particles were carried downstream due to a higher velocity and therefore were not able to diffuse onto the post surface in the high-velocity region.

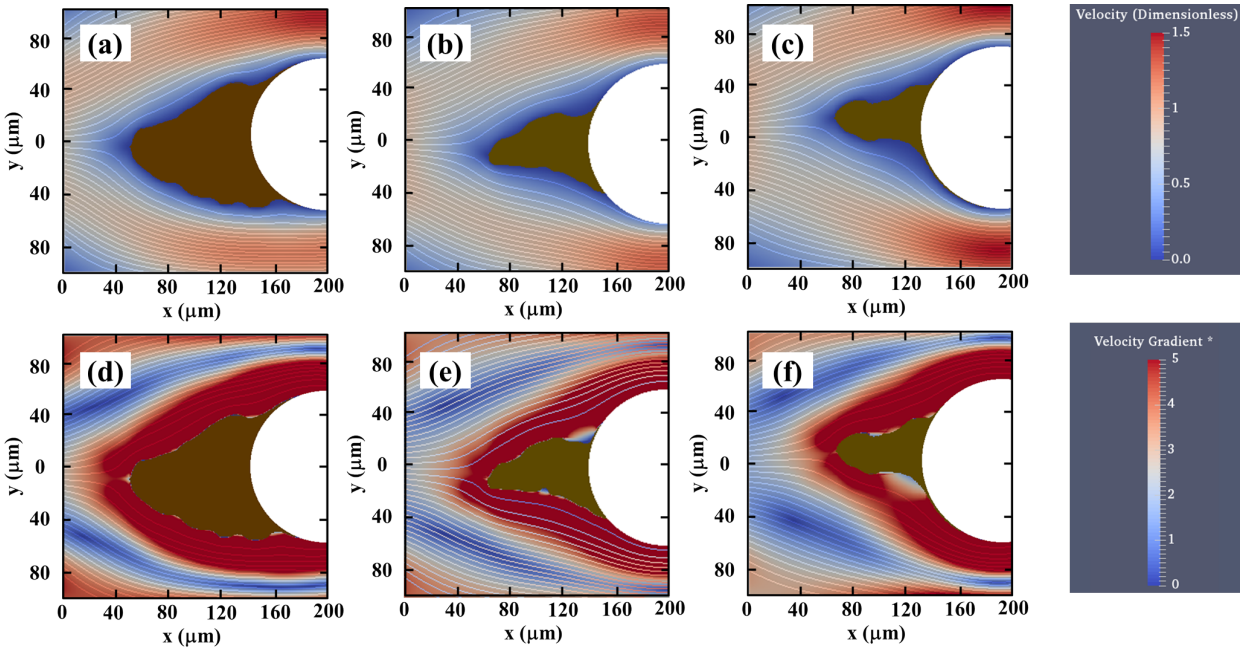

Figure 6: Velocity profiles and shear rate around representative asphaltene deposits at 50, 55 and 60 vol% heptane. Velocity profile: (a) 50 vol%, (b) 55 vol%, and (c) 60 vol%. Shear rate: (d) 50 vol%, (e) 55 vol%, and (f) 60 vol%. White area is the post. Brown area is the deposit.

Conclusions

The effect of asphaltene solubility on deposition was examined using porous media microfluidic devices. We demonstrated that the deposition dynamics varied significantly with different concentrations of heptane (a well-characterized asphaltene precipitant). We associated the differences in deposition profiles to changes in the particle size distribution with the corresponding Péclet number at varying heptane concentrations. Finally, we analyzed the results obtained by pore-scale visualization with the velocity profiles and shear rate near the deposit to better understand the effect of deposited asphaltenes on depositing ones. Once the deposit was formed, the deposits tended to grow against the flow direction (low-shear zone) rather than laterally (high-shear zone).

To solve asphaltene problems, a fundamental understanding of asphaltene behaviors at the micro-scale is needed. Well-defined mechanisms governing deposition can be further incorporated into deposition simulators to accurately predict flow assurance problems and guide the design of remediation strategies.

Acknowledgments

We acknowledge the financial support provided by the Abu Dhabi National Oil Company (ADNOC), the Abu Dhabi Oil R&D Sub-Committee, and the Petroleum Institute (PI), U.A.E. We thank Sun Young Ji and Sang Hun Ji for their technical support.

References

(1) Kokal, S. L.; Sayegh, S. G. Asphaltenes: The Cholesterol Of Petroleum; Society of Petroleum Engineers, 1995.
(2) Creek, J. L. Freedom of Action in the State of Asphaltenes: Escape from Conventional Wisdom. *Energy Fuels* **2005**, *19* (4), 1212–1224.
(3) Vargas, F. M.; Gonzalez, D. L.; Creek, J. L.; Wang, J.; Buckley, J.; Hirasaki, G. J.; Chapman, W. G. Development of a General Method for Modeling Asphaltene Stability. *Energy Fuels* **2009**, *23* (3), 1147–1154.
(4) Hirschberg, A.; deJong, L. N. J.; Schipper, B. A.; Meijer, J. G. Influence of Temperature and Pressure on Asphaltene Flocculation. *Soc. Pet. Eng. J.* **1984**, *24* (3), 283–293.
(5) Li, Z.; Firoozabadi, A. Modeling Asphaltene Precipitation by *N* -Alkanes from Heavy Oils and Bitumens Using Cubic-Plus-Association Equation of State. *Energy Fuels* **2010**, *24* (2), 1106–1113.
(6) Buckley, J. S.; Hirasaki, G. J.; Y. Liu; S. von Drasek; J-X. Wang; B.S. Gill. Asphaltene Precipitation and Solvent Properties of Crude Oils. *Pet. Sci. Technol.* **1998**, *16* (3–4), 251–285.
(7) Wang, J.; Buckley, J. S.; Creek, J. L. Asphaltene Deposition on Metallic Surfaces. *J. Dispers. Sci. Technol.* **2004**, *25* (3), 287–298.
(8) Mullins, O. C.; Sabbah, H.; Eyssautier, J.; Pomerantz, A. E.; Barré, L.; Andrews, A. B.; Ruiz-Morales, Y.; Mostowfi, F.; McFarlane, R.; Goual, L.; et al. Advances in Asphaltene Science and the Yen–Mullins Model. *Energy Fuels* **2012**, *26* (7), 3986–4003.
(9) Buckley, J. S. Asphaltene Deposition. *Energy Fuels* **2012**, *26* (7), 4086–4090.
(10) Nabzar, L.; Aguiléra, M. E. The Colloidal Approach. A Promising Route for Asphaltene Deposition Modelling. *Oil Gas Sci. Technol. - Rev. IFP* **2008**, *63* (1), 21–35.
(11) Hoepfner, M. P.; Limsakoune, V.; Chuenmeechao, V.; Maqbool, T.; Fogler, H. S. A Fundamental Study of Asphaltene Deposition. *Energy Fuels* **2013**, *27* (2), 725–735.
(12) Hashmi, S. M.; Loewenberg, M.; Firoozabadi, A. Colloidal Asphaltene Deposition in Laminar Pipe Flow: Flow Rate and Parametric Effects. *Phys. Fluids* **2015**, *27* (8), 083302.
(13) Lawal, K. A.; Crawshaw, J. P.; Boek, E. S.; Vesovic, V. Experimental Investigation of Asphaltene Deposition in Capillary Flow. *Energy Fuels* **2012**, *26* (4), 2145–2153.
(14) Boek, E. S.; Ladva, H. K.; Crawshaw, J. P.; Padding, J. T. Deposition of Colloidal Asphaltene in Capillary Flow: Experiments and Mesoscopic Simulation. *Energy Fuels* **2008**, *22* (2), 805–813.
(15) Chaisoontornyotin, W.; Haji-Akbari, N.; Fogler, H. S.; Hoepfner, M. P. Combined Asphaltene Aggregation and Deposition Investigation. *Energy Fuels* **2016**, *30* (3), 1979–1986.
(16) Zhuang, Y.; Goharzadeh, A.; Lin, Y. J.; Yap, Y. F.; Chai, J. C.; Mathew, N.; Vargas, F.; Biswal, S. L. Three Dimensional Measurements of Asphaltene Deposition in a Transparent Micro-Channel. *J. Pet. Sci. Eng.* **2016**, *145*, 77–82.
(17) Vargas, F. M.; Creek, J. L.; Chapman, W. G. On the Development of an Asphaltene Deposition Simulator. *Energy Fuels* **2010**, *24* (4), 2294–2299.
(18) Jafari Behbahani, T.; Ghotbi, C.; Taghikhani, V.; Shahrabadi, A. Investigation of Asphaltene Adsorption in Sandstone Core Sample during CO2 Injection: Experimental and Modified Modeling. *Fuel* **2014**, *133*, 63–72.
(19) Ma, K.; Liontas, R.; Conn, C. A.; Hirasaki, G. J.; Biswal, S. L. Visualization of Improved Sweep with Foam in Heterogeneous Porous Media Using Microfluidics. *Soft Matter* **2012**, *8* (41), 10669–10675.
(20) Conn, C. A.; Ma, K.; Hirasaki, G. J.; Biswal, S. L. Visualizing Oil Displacement with Foam in a Microfluidic Device with Permeability Contrast. *Lab. Chip* **2014**, *14* (20), 3968–3977.
(21) Bowden, S. A.; Wilson, R.; Parnell, J.; Cooper, J. M. Determination of the Asphaltene and Carboxylic Acid Content of a Heavy Oil Using a Microfluidic Device. *Lab. Chip* **2009**, *9* (6), 828–832.
(22) Sieben, V. J.; Tharanivasan, A. K.; Ratulowski, J.; Mostowfi, F. Asphaltenes Yield Curve Measurements on a Microfluidic Platform. *Lab Chip* **2015**, *15* (20), 4062–4074.

(23) Hu, C.; Morris, J. E.; Hartman, R. L. Microfluidic Investigation of the Deposition of Asphaltenes in Porous Media. *Lab. Chip* **2014**, *14* (12), 2014–2022.
(24) Hu, C.; Hartman, R. L. High-Throughput Packed-Bed Microreactors with in-Line Analytics for the Discovery of Asphaltene Deposition Mechanisms. *AIChE J.* **2014**, *60* (10), 3534–3546.
(25) Spiecker, P. M.; Gawrys, K. L.; Trail, C. B.; Kilpatrick, P. K. Effects of Petroleum Resins on Asphaltene Aggregation and Water-in-Oil Emulsion Formation. *Colloids Surf. Physicochem. Eng. Asp.* **2003**, *220* (1–3), 9–27.
(26) Hoepfner, M. P.; Vilas Bôas Fávero, C.; Haji-Akbari, N.; Fogler, H. S. The Fractal Aggregation of Asphaltenes. *Langmuir* **2013**, *29* (28), 8799–8808.
(27) Tavakkoli, M.; Panuganti, S. R.; Vargas, F. M.; Taghikhani, V.; Pishvaie, M. R.; Chapman, W. G. Asphaltene Deposition in Different Depositing Environments: Part 1. Model Oil. *Energy Fuels* **2014**, *28* (3), 1617–1628.
(28) Tavakkoli, M.; Grimes, M. R.; Liu, X.; Garcia, C. K.; Correa, S. C.; Cox, Q. J.; Vargas, F. M. Indirect Method: A Novel Technique for Experimental Determination of Asphaltene Precipitation. *Energy Fuels* **2015**, *29* (5), 2890–2900.
(29) Hildebrand, J. H.; Wood, S. E. The Derivation of Equations for Regular Solutions. *J. Chem. Phys.* **1933**, *1* (12), 817–822.
(30) Wiehe, I. A.; Kennedy, R. J. The Oil Compatibility Model and Crude Oil Incompatibility. *Energy Fuels* **2000**, *14* (1), 56–59.
(31) Haji-Akbari, N.; Masirisuk, P.; Hoepfner, M. P.; Fogler, H. S. A Unified Model for Aggregation of Asphaltenes. *Energy Fuels* **2013**, *27* (5), 2497–2505.
(32) Wang, J. X.; Buckley, J. S. A Two-Component Solubility Model of the Onset of Asphaltene Flocculation in Crude Oils. *Energy Fuels* **2001**, *15* (5), 1004–1012.
(33) Wägli, P.; Homsy, A.; de Rooij, N. F. Norland Optical Adhesive (NOA81) Microchannels with Adjustable Wetting Behavior and High Chemical Resistance against a Range of Mid-Infrared-Transparent Organic Solvents. *Sens. Actuators B Chem.* **2011**, *156* (2), 994–1001.
(34) Hung, L.-H.; Lin, R.; Lee, A. P. Rapid Microfabrication of Solvent-Resistant Biocompatible Microfluidic Devices. *Lab. Chip* **2008**, *8* (6), 983–987.
(35) Xia, Y.; Whitesides, G. M. Soft Lithography. *Angew. Chem. Int. Ed.* **1998**, *37* (5), 550–575.
(36) Penberthy, W. L.; Shaughnessy, C. M. *Sand Control*; Series on special topics ; Henry L. Doherty series; Henry L. Doherty Memorial Fund of AIME, Society of Petroleum Engineers: Richardson, TX, 1992.
(37) Schneider, C. A.; Rasband, W. S.; Eliceiri, K. W. NIH Image to ImageJ: 25 Years of Image Analysis. *Nat. Methods* **2012**, *9* (7), 671–675.
(38) Hunter, J. D. Matplotlib: A 2D Graphics Environment. *Comput. Sci. Eng.* **2007**, *9* (3), 90–95.
(39) Otsu, N. A Threshold Selection Method from Gray-Level Histograms. *IEEE Trans. Syst. Man Cybern.* **1979**, *9* (1), 62–66.
(40) Kusaka, Y.; Duval, J. F. L.; Adachi, Y. Morphology and Breaking of Latex Particle Deposits at a Cylindrical Collector in a Microfluidic Chamber. *Environ. Sci. Technol.* **2010**, *44* (24), 9413–9418.
(41) Vincent, M. R. de S.; Abkarian, M.; Tabuteau, H. Dynamics of Colloid Accumulation under Flow over Porous Obstacles. *Soft Matter* **2016**, *12* (4), 1041–1050.
(42) Eskin, D.; Ratulowski, J.; Akbarzadeh, K.; Pan, S. Modelling Asphaltene Deposition in Turbulent Pipeline Flows. *Can. J. Chem. Eng.* **2011**, *89* (3), 421–441.